Two-Photon Thermal Bleaching of Single Fluorescent Molecules

Giuseppe Chirico,* Fabio Cannone,* Giancarlo Baldini,* and Alberto Diaspro†
*Istituto Nazionale per la Fisica della Materia, U.d.R. Milano-Bicocca, Via Cozzi 52, 20126, Milan, Italy and †Instituto Nazionale per la Fisica della Materia, U.d.R. Genova, Via Dodecaneso 33, 16146, Genoa, Italy

ABSTRACT We have studied the fluorescence emission by two-photon excitation of four dyes widely used for bioimaging studies, rhodamine 6G, fluorescein, pyrene and indo-1 at the single molecule level. The single dye molecules, spread on a glass substrate by spin coating, show a constant fluorescence output until a sudden transition to a dark state very close to the background. The bleaching time that is found to vary in the series pyrene, indo-1, fluorescein and rhodamine 6G from the fastest to the slowest one respectively, has a Gaussian distribution indicating that the observed behavior is not due to photobleaching. Moreover, the bleaching time decreases with the glass substrate temperature reaching a vanishing nonmeasurable value for a limiting temperature whose value is found in the same series as for the bleaching time, from the lowest to the highest temperature respectively. The observed bleaching shows a clear correlation to the amount of absorbed power not reirradiated as fluorescence and to the complexity of the molecule. These observations are interpreted as thermal bleaching where the temperature increase is induced by the two-photon absorption of the single dyes as confirmed also by numerical simulations.

INTRODUCTION

Single molecule spectroscopy requires often the immobilization of the molecules onto solid substrates and the use of relatively high excitation intensity obtained through single photon confocal microscopy (Garcia-Parajo et al., 2000; Lu and Xie, 1997; Pierce et al., 1997; Xu and Young, 1988) or two-photon excitation microscopy (Sanchez et al., 1997; Chirico et al., 2001). Single molecule spectroscopy is generally characterized by blinking due to the intersystem crossing (Veerman et al., 1999; Garcia-Parajo et al., 2000) or the conversion to differently protonated states (Weber et al., 1999; Zumbusch and Jung, 2000). The on-off switching of blinking typically occurs in the time scale of milliseconds (Garcia-Parajo et al., 2000). For single photon excitation, the sudden irreversible loss of fluorescence from single molecules was ascribed tentatively either to photo- or thermally induced bleaching. On the other hand, although two-photon excitation has several advantages for the spectroscopic and imaging applications (Denk et al., 1990; Diaspro, 2002), little is known about similar effects on the stability of the molecules. The studies in the literature mostly refer to bulk measurements. Mertz (1998) has compared the single to two-photon excitations with particular regard to the saturation or higher levels transitions. More recently a work by Patterson and Piston (2000) has provided data on bulk solutions of dyes that indicate an enhanced photobleaching in two-photon spectroscopy due probably to a three-photon process.

Several definitions of bleaching can be given (Song et al., 1995; 1996), and we can envision two main sources. The molecule may convert from the excited state, usually with a radiative decay constant in the tens of nanoseconds range, to a second excited metastable state with vanishing radiative constant. Irreversible photobleaching and blinking are usually ascribed to this type of transition. Another possibility is that the molecule changes its structure in such a way that the molecular ground state assumes a vanishing cross section for the excitation light. This modification may be induced by isomerization or thermal absorption. In both cases the molecular fluorescence emission drops to zero.

It is the primary aim of the present work to assess the effect of two-photon excitation on the total amount of fluorescence that can be collected from a single immobilized molecule at the high excitation intensities required for single molecule studies with two-photon excitation. To this purpose we have considered four dyes, namely: indo-1, rhodamine 6G, fluorescein, and pyrene. For these molecules we have evaluated the total amount of fluorescence light that can be recovered from each dye versus the excitation intensity, the temperature, the duration, and the nature of the excitation. The choice of these dyes is motivated also by the different complexity of the chemical structure that increases from pyrene to indo-1. The main result of this research is the characterization of the thermally induced bleaching of the dyes and a clear correlation of the bleaching time and its dependence on the excitation intensity, with the photophysics parameters of the molecules. These conclusions will be based also on numerical simulations of the local temperature increase during laser excitation.

MATERIALS AND METHODS

Optical setup

The laser source is a mode-locked Ti:sapphire laser (Tsunami 3960, Spectra Physics, Mountain View, CA) pumped by a solid state laser at 532 nm (Millennia V, Spectra Physics) that produces pulses with ≅100 fs full-width at half maximum (FWHM) at a repetition frequency of 80 MHz and has an average power output ≅700 mW at $\lambda = 770$ nm. The optical setup is built

Submitted May 16, 2002, and accepted for publication July 10, 2002.

Address reprint requests to Giuseppe Chirico, Dept. of Physics, University of Milan-Bicocca, 20126 Milan, Italy. Tel: 39-02-64482872; Fax: 39-02-64482894; E-mail: giuseppe.chirico@mib.infn.it.

0006-3495/03/01/588/11 $2.00

around an inverted microscope (TE300, Nikon, Firenze, Italy) and a PCM2000 Nikon scanning head. A portion of the laser beam is focused at the entrance of the PCM2000 by a plano-convex lens with a numerical aperture of 0.15, passes through a dichroic mirror (650 DCSPRX C72-38; Chroma Inc., Brattleboro, VT) and is sent to the entrance pupil of the objective ($N.A. = 1.4$, Plan Apochromat 100X oil, Nikon, Firenze, Italy) by the scanning lens. The laser power at the object plane can be adjusted by means of neutral filters; we estimate that ≅30% of the laser light entering the scanning head is actually exciting the sample due to losses and absorption of the light mainly in the objective. The fluorescence signal, collected by the same objective and selected by a filter (HQ535-50, Chroma Inc., Brattleboro, VT), is fed to a multimode fiber that brings the light to a photomultiplier (R928, Hamamatsu, Milan, Italy) in the PCM2000 controller (Diaspro, 2001).

Sample preparation

The rhodamine 6G solutions have been prepared by dissolving rhodamine 6G (Fluka Chemika, Milan, Italy, Cat. No. 83698) in dimethylsulfoxide (DMSO) at a concentration ≅100 μM. The fluoresceine solutions have been prepared by dissolving fluoresceine (Fluka Chemika, Cat. No. 46955) in TRIS buffer at a concentration ≅100 μM. The glass slides are spin coated with solutions obtained by diluting the DMSO-rhodamine and the TRIS-fluoresceine concentrated stocks in ethanol at concentrations ≅70–300 nM. The Pyrene solutions have been prepared by dissolving pyrene powder (Fluka Chemika, Cat. No. 82650) in DMSO at a concentration ≅100 μM. The Indo-1 solutions have been prepared by dissolving Indo-1 powder (Fluka Chemika, Cat.No. 57180) in MilliQ water (Millipore S.p.a., Milano, Italy).

Glass slides cleaning

The glass slides have been soaked first in a 1% sodium dodicyl-sulfate (for 24 h), then in a saturated methanol solution of NaOH (for 2 h). We have then employed a two-step protocol to remove NaOH. We first soaked the slides in a 0.1% HCl solution for 2 h and then in diluted chromic solution (KCr_2 in concentrated phosphoric acid) for 2 h. The glasses were then stored in ethanol and finally rinsed thoroughly with MilliQ water (Millipore S.p.a., Milano, Italy) and dried with nitrogen flow just before the fluorescent solutions were spread on the glass slide by spin coating.

Imaging of the slides

The fluorescence emitted from the slides is imaged by the Nikon EZ-2000 software interfaced to the PCM2000 scanning head (Diaspro et al., 2001). The point spread function of the setup has been measured elsewhere and corresponds to a plane resolution of ≅0.21 μm and an axial resolution of ≅0.7 μm (Diaspro et al., 1999). The acquisition of the images (160 × 160 pixels) with residence times in the range 9.6 μs per pixel takes ≅0.24 s. The field of view employed is in the range 10–15 μm and the excitation power is usually ≅15–45 mW at the entrance of the scanning head, unless otherwise explicitly stated. With our estimate that only ≅30% of the laser light actually impinges on the sample, the light intensity is ≅1000–3000 kW/cm^2. We report the estimated values of the power at the sample in the results. The temperature of the slides is kept at the desired temperature by thermostating a copper ring at contact with the cover slip. Most of the measurements have been performed at room temperature, $T \cong 21.0$°C. The images were taken by exciting at the wavelengths $\lambda = 770$ nm for rhodamine 6G and fluorescein, and $\lambda = 720$ nm for pyrene and indo-1.

Fluorescence kinetics of the spots

We have taken sequential images for a total time of ≅100 s. The fluorescence intensity of each spot has been computed by summing the pixel content in a circular area around each spot and by normalizing for the number of pixels in this area that have a typical diameter of ≅10 pixels. The maximum illumination time per spot is therefore ≅1 ms for a residence time ≅9.6 μs, and can be estimated from the time needed to scan an area of 10 × 10 pixels on the 160 × 160 image. The time per image is 229 ms and corresponds to the time interval between the subsequent illumination of each molecule. The data reported in the Results section have been shown versus the time interval between subsequent images.

The stability of the microscope stage in the z-direction has been assessed by taking two 140 × 140 μm^2 images right before and after the kinetics on a 10–15 μm field of view, and by verifying that only the spot on which the kinetics was performed was missing in the second 140 × 140 μm^2 image. We checked also for the stability of the acquisition module (Hamamatsu photomultipliers, R928), by imaging a DC-biased green light emitting diode and performing long-term kinetics as done for the studies of the dyes. The stability of the signal was found to be ≅0.4% on a 100 s kinetics.

The computation of the total intensity of a spot is made by means of home-coded MathLab (Mathworks, Torino, Italy) programs that allow also to identify a single spot on a time series of images and to compute the spot intensity versus the acquisition time (Chirico et al., 2001).

Fluorescence histograms on images

Single snapshot images showed typically several distinct spots ascribed to fluorescence signal from either single dyes or small aggregates (Fig. 1). To assess the aggregation number of each spot a histogram analysis of the fluorescence output was performed on the first image of each fluorescence kinetics series. We always obtained histograms with discrete peaks corresponding to a fluorescence output linearly spaced and indicating the presence of aggregates of different order. A typical result is shown in Fig. 1.

RESULTS

Fluorescence kinetics versus the excitation power: single molecules

Before investigating the fluorescence kinetics we studied the trend of the fluorescence signal per single molecule versus

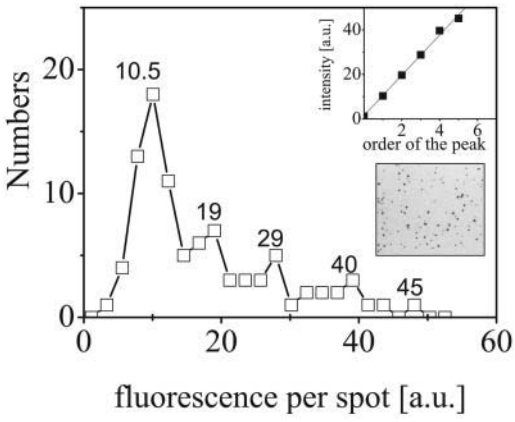

FIGURE 1 Distribution of the intensity of the spots of an image of a glass slide prepared by spin coating a $C = 11.8$ μM Indo-1 solution. The image was acquired with residence time ≅3 μs, 97 × 97 μm field of view and excitation power ≅10.5 mW. The numbers on top of the peaks of the distribution indicate the approximate fluorescence level. Upper inset: Fluorescence of the peaks in the distribution in order of increasing intensity. The background level acquired on the same image far from any visible spot ≅ 900 ± 130 arbitrary units, has been subtracted from the data. Lower inset: typical fluorescence image of the spin coated glasses.

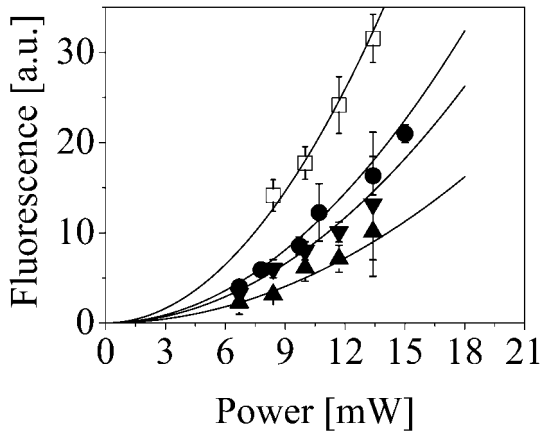

FIGURE 2 Fluorescence signal (arbitrary units) per single molecule versus the excitation power. The average has been computed on at least 80 molecules. The symbols indicate Fluorescein (▼), Rhodamine 6G (●), Pyrene (▲), and Indo-1 (□). The data are fit to a law of the type $A_{EXC} \times P^2$. The parameter A_{EXC} is reported in Table 1.

the average excitation power, $\langle P \rangle_{ave}$. All the data, collected between 3.4 and 13.4 mW are always well described by a second power law, as shown in Fig. 2. The best fit to a law of the kind $A_{EXC} \times \langle P \rangle^2_{ave}$ gives the values of A_{EXC} reported in Table 1.

We have then followed the fluorescence emission of several (≅80) single dyes and small aggregates at different excitation intensities. For single dyes the fluorescence remains relatively constant until a sudden drop to a value very close to the background level from the glass slide occurs (Fig. 3). The time at which the transition occurs is evaluated by fitting the fluorescence output to a sigmoid function and by taking the middle transition time, T_B. The bleaching rate, Γ_B, defined as the inverse of this time, has a distribution very close to a Gaussian with a small width (typically 6%; see the inset of Fig. 3). This clearly indicates that the process leading to the loss of fluorescence is not photobleaching, because an exponential distribution should be found in this case (Garcia-Parajo et al., 2000; Veerman et al., 1999). On the other hand, the observed bleaching does depend on the excitation power, $\langle P \rangle_{ave}$, as shown in Fig. 4 for all the four dyes investigated. The trend of the data is well described by a power law of the type, $B \times \langle P \rangle^C_{ave}$ and the values of the best fit parameters are reported in Table 1. The value of the power exponent is found in the range $2.1 < C < 2.6$ in the series pyrene < Indo-1 < fluorescein < rhodamine.

Fluorescence kinetics versus the excitation power: aggregates

When following the fluorescence kinetics of the aggregates we found a multistep decrease of the signal as shown in Fig. 5. The number of steps was consistent with the aggregation order as evaluated from the histogram analysis (for an aggregate of order N we observed a number of fluorescence drops $\leq N$). Moreover the fluorescence drop per step was always very close to the quantum of fluorescence per molecule measured on the histograms. The bleaching times $t_{N,n}$ of an aggregate of order N were defined as the time corresponding to the nth drop of fluorescence signal. For each aggregate and excitation power, we found that the average value $T_{BN} = \sum_{n=1...N} t_{N,n}/N$ lies very close to T_B. By forcing the fit of the fluorescence kinetics for the aggregates to a single exponential decay, $\exp[-t/\xi_N]$, we obtained an average time decay constant, ξ_N, which is approximately linearly dependent on the aggregation number $\xi_N = N\xi_0$ (see inset of Fig. 5). The slopes ξ_0 for the four dyes at $P = 10$ mW are reported in Table 1.

Recovery of the fluorescence after bleaching

For rhodamine 6G, fluorescein, and indo-1, we found that a percentage (see Table 1) of the single molecules investigated, recovered the fluorescence signal after the bleaching as shown in Fig. 3. For pyrene, no recovery after bleaching was observed for the samples and the observation times employed here. The time span when no fluorescence signal was observed, T_D, was found slightly dependent on the excitation power (data not shown) and the average values are $T_D = 34 \pm 2$ s for fluorescein, $T_D = 43 \pm 3$ s for rhodamine 6G and $T_D = 59 \pm 3$ s for indo-1. The percentage of the molecules that showed a recovery after bleaching showed a marked dependence on the excitation power as

TABLE 1 Best fit parameters and photophysical parameters for the dyes

Dye	A_{EXC}	$B \times 10^4$	C	ξ_0 [s]	B_R	R_F%	δ_2 [GM]	ϕ
Fluorescein	0.081	0.49 (0.05)	2.45 (0.01)	1.1 (0.1)	1.8 (0.7)	20%	38 ± 9 {at pH > 9}	0.9 (0.05)
Rhodamine 6G	0.1	0.19 (0.01)	2.62 (0.3)	1.85 (0.1)	2.70 (0.07)	27%	100 ± 55 {methanol}	0.95 (0.05)
Pyrene	0.055	4 (1)	2.1 (0.02)	0.34 (0.06)	0.22 (0.01)	0%	—	0.6
Indo-1	0.21	2.9 (0.2)	2.2 (0.6)	0.29 (0.06)	0.28 (0.02)	13%	12 {water}	0.9

First column: Best fit parameters of the fluorescence signal per single molecule versus the excitation power $= A_{EXC}P^2$. Second and third columns: best fit parameters of the bleaching rate Γ_B versus the excitation power $\Gamma_B = BP^C$. Fourth column: the slope ξ_0 of the effective decay time of the aggregate kinetics versus the aggregation order at $P = 10$ mW. Fifth column: the slope of the retarded bleaching time T_{BR} versus the dark time, τ_D according to the fit $T_{BR} = A_R + B_R{}^*\tau_D$; Sixth column: the percentage of the fluorescence recovery at $P = 10$ mW; Seventh column: the two-photon cross section $\delta_2 \times 10^{50}$[cm^{4}s^2/photons] taken from Xu and Webb (1996); Eighth column: the quantum yield ϕ (taken from Demas and Crosby (1971) and Haughland (1996)). The numbers in round parentheses are the standard errors of the data. The measurement conditions for the cross section are indicated in curled parentheses.

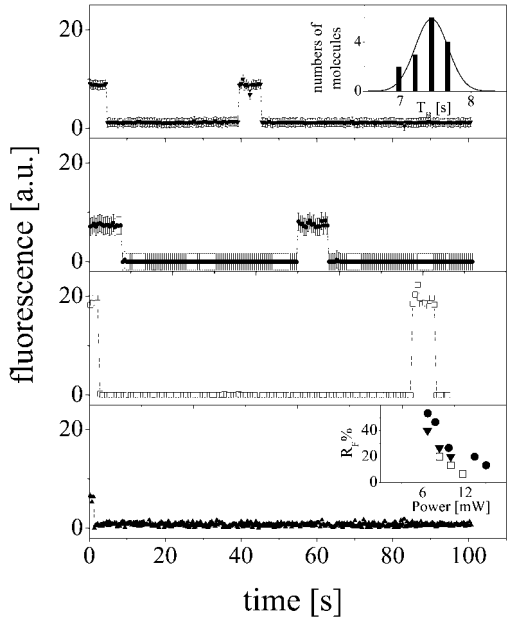

FIGURE 3 Typical fluorescence signal versus time for single molecules of Fluorescein (▼ *top panel*), Rhodamine 6G (●, *second panel from top*), Indo-1 (□, *third panel from top*) and Pyrene (▲, *bottom panel*) at 6.7 mW of excitation power. Inset right top: typical distribution of the bleaching time for Fluorescein. Inset right bottom: percentage, R_F%, of the single molecules that show fluorescence recovery after bleaching versus the excitation power for fluorescein, rhodamine 6G and indo-1. Symbols are the same as in the main panels.

shown in the lower inset of Fig. 3. Within the time window of our acquisitions, we observed a second bleaching of the recovered fluorescence signal after a time T_{DB}, that depends on the excitation power. The corresponding bleaching rate, $\Gamma_{DB} = T_{DB}^{-1}$, was found close to Γ_B within 10%, at most (data not shown).

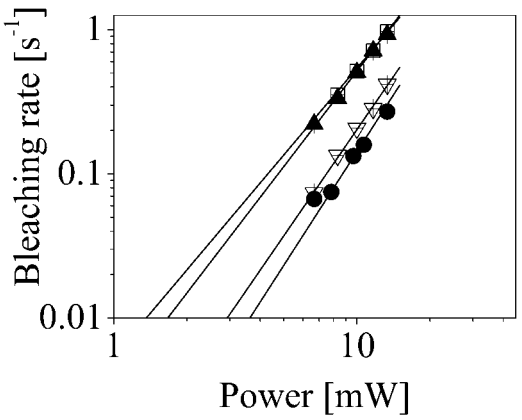

FIGURE 4 Average Bleaching rate, Γ_B, of Rhodamine6G (●), Fluorescein (▼), Indo-1 (□) and Pyrene (▲), versus the excitation power. The solid lines are fits to a power law, $B \times P^C$; the best fit values of B and C are reported in Table 1.

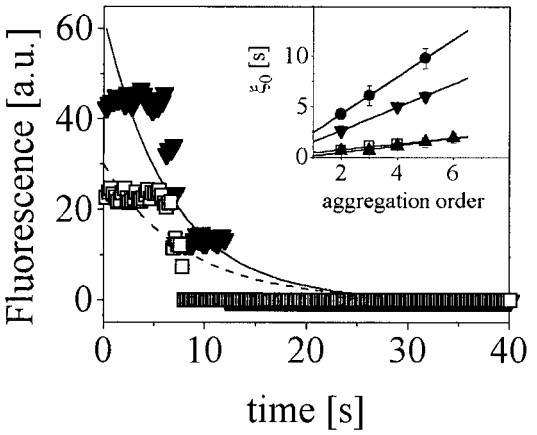

FIGURE 5 Typical fluorescence kinetics for aggregates of rhodamine 6G molecules: a fourth order aggregate (▼) and a second order aggregate (□). Solid and dashed lines are the best fit to an exponential decay for the fourth and the second order aggregate kinetics, respectively. Inset: average decay time obtained by fitting the aggregate kinetics to a single exponential decay, ξ_N, versus the order of aggregation for Fluorescein (▼), Rhodamine 6G (●), Pyrene (▲), and Indo-1 (□). The solid lines are the linear fits, $\xi_N = N\,\xi_0$. The values of ξ_0 for the four dyes are reported in Table 1.

Fluorescence kinetics with intermittent excitation

The observed dependence of the bleaching rates on the excitation power could be related to the integral of the absorbed power or to the way the molecules are illuminated. To discriminate between these two possibilities, we studied the fluorescence kinetics from single dyes with intermittent excitation. Three fluorescence images were collected from the sample for a total illumination of $\tau_I = 3 \times 229$ ms and then the laser light was blocked for a variable interval τ_D after which the sample was again imaged for τ_I. This illumination sequence was repeated for a total acquisition time > 100 s (see Fig. 6). As observed in Fig. 6 for the example of rhodamine 6G, the emission of fluorescence continued up to a time T_B^*. This behavior was found for all the four dyes. We computed an effective bleaching time, T_{BR}, as the total time for which the molecules were illuminated and emitting: $T_{BR} = T_B^* - (n-1)\tau_D$. For each dye T_{BR} increases with τ_D and the data are well described by a linear law (see Fig. 6, *right panel*), $T_{BR} = A_R + B_R{}^*\tau_D$, where A_R is found close to $T_B = 1/\Gamma_B$ (within 10%), and B_R varies accordingly to the molecule as reported in Table 1.

Fluorescence kinetics versus substrate temperature

The dependence of the bleaching time on the duration of the intervening dark periods may suggest an absorption effect that could lead to a temperature increase of the sample or the substrate. If this occurs, the fluorescence kinetics should be dependent on the substrate temperature. Therefore the time kinetics of the single dyes was followed versus the substrate

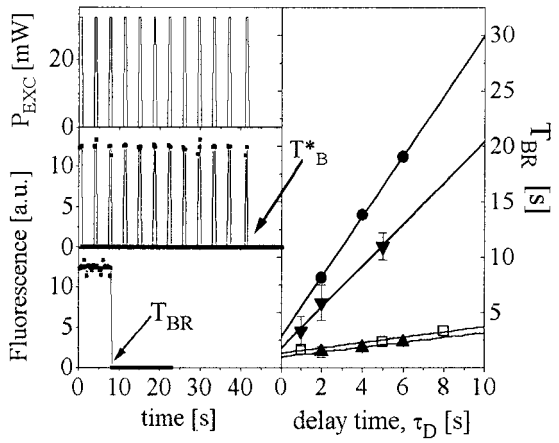

FIGURE 6 Left panels: scheme of the intermittent excitation experiments. These data refer to a single rhodamine 6G molecule with excitation ≅10.7 mW. Upper left panel: Excitation power versus time: the excitation power is null for a time τ_D. Middle left panel: Fluorescence signal as recovered from the analysis of all images. In the panel, the T_B^* ($T_B^* = 41.7$ s for this case) is indicated with an arrow. Lower left panel: Fluorescence signal reconstructed by dropping the intervals when the sample was not illuminated. In the panel the T_{BR} ($T_{BR} = 8.9$ s for this case) is indicated with an arrow. Right panel: Bleaching time with intermittent excitation versus the delay time τ_D for rhodamine 6G (●) fluorescein (▼), indo-1 (□), and pyrene ▲. The solid lines are linear fit to the data: $T_{BR} = A_R + B_R\tau_D$. The best fit parameter B_R is reported in Table 1.

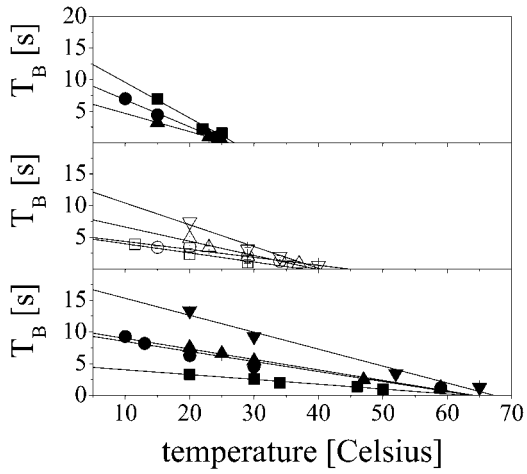

FIGURE 7 Bleaching times versus the substrate temperature for: indo-1 (*top panel*, excitation powers 10, 8.4, 7.8 mW from the bottom to the top curve); fluorescein (*middle panel*, excitation powers 11.7, 10, 8.4, 5.7 mW from the bottom to the top curve); rhodamine 6G (*bottom panel*, excitation powers 13.4, 10.7, 9.7, 7.8 mW from the bottom to the top curve).

temperature for different values of the excitation power. As reported in Fig. 7 the bleaching time was found to decrease versus the temperature with a slope that depends on the excitation power. Moreover, the bleaching time was found for each dye to intersect the temperature axis at a definite value of temperature T_0, approximately independent of the excitation powers investigated (see Fig. 7). The average values of T_0 taken over the sets of excitation powers are: $T_0 = 64.6 \pm 1.8$°C for rhodamine 6G, $T_0 = 40.7 \pm 3$°C for fluorescein and $T_0 = 26.4 \pm 0.5$°C for indo-1. The fast bleaching of pyrene at room temperature did not allow to study its temperature dependence.

DISCUSSION

In the measurements reported here, we observed fluorescence spots that can be ascribed to the emission from single molecules or small aggregates according to the histogram analysis reported in the Materials and Methods section and in Fig. 1. The dependence of the single molecule fluorescence output on the square of the excitation power indicates (see Fig. 2) that a two-photon excitation is taking place. No evidence for saturation effects was detected for the dyes investigated here indicating that the two-photon saturation power must be larger than ≅10 mW corresponding to ~3000 kW/cm^2 similarly to the data reported by Brand et al. (1997) on coumarin-120 in solution. Because the saturation intensity for pulsed excitation (with pulse width much less than excited state lifetime) is proportional to $(\delta_2\tau_p)^{0.5}$ we can estimate an intensity saturation of ~14,000 kW/cm^2 for a typical two-photon cross section of $\delta_2 = 50$ GM and a laser pulse width $\tau_p = 100$ fs. This saturation value is ~4–5 times larger than the maximum intensity reached here. On the other hand the absence of saturation evidence in the data reported in Fig. 2 may indicate that the cross sections of the investigated dyes, when on glass, is lower than in solution. The emission of fluorescence from single molecules or small aggregates fluctuates around an average value until a single or multistep drop to the background level as shown in Fig. 3.

Before making considerations on the fluorescence kinetics, we have checked that the reported behavior does not depend on the optical setup. The stability of the microscope stage in the z-direction and the stability of the acquisition module were assessed as described in the Materials and Methods section. We considered also molecular diffusion or sublimation as a possible explanation of the fluorescence loss, alternative to the changes in the photophysical parameters of the molecules. However this does not seem to be the case (Wahl, 1996) because the molecules were immobilized on the surface of the glass by physisorption and similar results as those reported here were found on samples sealed with a glass slide on the top (data not shown). The observed photobleaching is not even due to artifacts related to the saturation of the ground state because the fluorescence intensity dependence on the excitation power is very well described by a quadratic law (see Fig. 2). The saturation is ruled by the excited state lifetime of the dyes on the glass substrate that is probably shorter than that measurable in the bulk solutions. By assuming an average lifetime ≅1 ns for the dyes, we can estimate that our experiments have been carried out with intensities about an order of magnitude below the saturation level. Likewise, any significant

variation of the ≅150-fs pulse-width as a function of power would also affect the fluorescence signal producing a discrepancy with the square law dependence.

A few observations can then be made on the fluorescence kinetics of the type reported in Fig. 3. First of all, the process leading to the loss of fluorescence is neither photobleaching nor blinking, because an exponential distribution of the off times (and on times) should be found for a stochastic process, while the distributions of the T_B that we recover from the data were very close to a Gaussian function (see inset in Fig. 3). This distribution of the bleaching times indicates that the phenomenon is not ruled by stochastic processes, such as the transition between excited electronic states.

Moreover the fluorescence emission is not continuous but interrupted by long dark intervals: in some cases the fluorescence is recovered within the 100 s observation window (see Fig. 3 and lower inset therein). The lifetime of the triplet state varies from few μs to tens of ms (Veerman et al., 1999), while the length of the dark periods observed by us is on the order of seconds. On the other hand the blinking due to the triplet-singlet interconversion (Dickson et al., 1997; Zumbusch and Jung, 2000; Song et al., 1996; Haupts et al., 1998; Schwille et al., 2000) is masked in our ≅250 ms acquisition time. Instead, our finding of emission intervals separated by dark periods suggests the existence of an additional (nonemissive) state B in the usual three-levels electronic system, S_0 (singlet ground state), S_1 (singlet excited state) and T_1 (triplet ground state). The state B might be characterized by a low two-photon cross section for the wavelengths used here, 720 nm–770 nm, or by a vanishing quantum yield.

On the basis of the results on the temperature dependence of the bleaching (see Fig. 7), we suggest that the silent state B may be related to a thermally induced structural change of the dyes. As indicated also by Walser et al. (2001) with line width and line shift measurements at cryogenic temperatures, one part of the laser power is absorbed by the single molecules and dissipated to the substrate. Within this hypothesis the common temperature value T_0, to which the curves of the bleaching time versus the substrate temperature are converging, should be closely related to the value at which the single dye undergoes the structural transition to the state B. For pyrene it was not possible to collect bleaching data at temperatures significantly higher than 21°C, room temperature, because the bleaching was rapidly increasing to a level where no fluorescence from single molecules could be collected.

Also the loss and recovery of fluorescence can be cast in this thermally induced transition picture if we assume that the B state is characterized by a very low cross section for the infrared (IR) radiation. In this case, the dark time should be the time needed for the molecule to lower the temperature and undergo a transition to the original S_0 state. As a partial check to this hypothesis we notice that the dark times, T_D, depends very little on the excitation power, typically $<10\%$ (data not shown). On the other hand the percentage of the molecules that recover fluorescence after T_D, decreases with the excitation power (see inset in Fig. 3) and this indicates that not all the molecules in the B state can find a way back to the S_0 state when the temperature reaches the initial value.

This thermal bleaching hypothesis must be compared to the theoretical predictions of the sample temperature increase. The previous estimates given in the literature for the temperature increase due to two-photon excitation microscopy experiments (Schönle and Hell, 1998; Denk et al., 1995), dealt with the very weak water single-photon absorption which corresponds to the first order cross section for water at 720–800 nm and is of the order of 10^{-24} cm^2, almost eight orders of magnitudes less than the resonant single-photon cross section for dyes in the visible. In a conventional two-photon excitation imaging the fluorescent labels are slowly diffusing through the excitation volume and the environment has a relatively high thermal conductivity ($\chi \cong \chi_{water}$). Therefore the temperature increase of the dye environment due to the two-photon absorption of the fluorophore is negligible (Schönle and Hell, 1998). However in experiments on single molecules immobilized on glass surfaces the molecule is continuously illuminated and a percentage of the absorbed power is dissipated into heat. We assume for simplicity that all the nonradiative deexcitation processes lead to an increase of the thermal vibrations, therefore the temperature increase should be proportional to $(1 - \phi)$, where ϕ is the quantum yield. As a matter of fact the energy loss due to the vibrational relaxation occurring in the excited state leads to an additional molecule temperature increase which should then be proportional to ϕ but we assume here that this contribution is negligible. The thermal dissipation occurs both in the air and in the glass slide in a way that is difficult to model. Because the thermal conductivity of glass is almost 100 times larger than that of air, we can estimate an upper and lower bound to the temperature increase, by computing it for the case in which the molecule dissipates either completely in air or in glass. Moreover the molecule is somehow hydrated because the measurements are not taken in dry air. This increases the effective size of the molecule that can be considered in any case as a point absorber of the laser power. To make an estimate, we suppose therefore that the molecule is located at the beam waist of the laser beam and that the thermal conductivity χ of the medium is uniform. The temperature increase, $\Delta T(\mathbf{r}, t)$, satisfies the diffusion equation:

$$\rho C_P \frac{\partial}{\partial t}\Delta T(\mathbf{r},t) = \chi \nabla^2 \Delta T(\mathbf{r},t) + f(\mathbf{r},t), \qquad (1)$$

where ρ is the mass density and C_P is the specific heat at constant pressure of the molecule (in cal/g°K). The source term, $f(\mathbf{r}, t)$, is the absorbed power per unit volume per laser pulse, that can be written for a two-photon absorption as:

$$f_{TPE}(\mathbf{r},t) = \delta_2\left(\frac{\langle P\rangle_{ave}}{h\nu_{exc}\tau_p\nu_L\pi w_0^2}\right)^2\frac{h\nu_{em}(1-\phi)}{V_m}i^2(\mathbf{r})b(t) = f_{0,TPE}i^2(\mathbf{r})b(t), \quad (2)$$

where δ_2 is the two-photon cross section of the molecule, $\langle P\rangle_{ave}$ is the average power, $i(\mathbf{r})$ is the normalized laser power profile and $b(t)$ is the time profile of the laser pulse. We assume that the laser pulses have a width of $\tau_p \cong 200$ fs and the laser repetition is $\nu_L = 80$ MHz. For a single photon excitation the source term is:

$$f_{OPE}(\mathbf{r},t) = \delta_1\left(\frac{\langle P\rangle_{ave}}{h\nu_{exc}\tau_p\nu_L\pi w_0^2}\right)\frac{h\nu_{em}(1-\phi)}{V_m}i(\mathbf{r})b(t) = f_{0,OPE}i(\mathbf{r})b(t), \quad (3)$$

where δ_1 is the single photon excitation. This can be the case of the hydration water layer excited by the IR radiation. The solution of the diffusion Eq. 1 for the two-photon absorption can be obtained by applying the Fourier transform as reported in the Appendix and Eq. 10 can be easily employed to perform a simulation of the effective increase in the local temperature. Because the contribution of C_P and ρ of the single hydrated dyes is small, we can simulate the temperature increase by assuming the density and the specific heat of water and the thermal conductivity either of the air, $\chi_{air} = 6 \times 10^{-6}$ Kcal/sm°K, or of the glass, $\chi_{glass} = 10^{-4}$ Kcal/sm°K.

Moreover, because the computations made above assume a three-dimensional Gaussian shape for the laser beam in the focus, we take $w_0 = 0.22$ μm and $z_0 = 0.66$ μm, that gives an excitation volume close to that of our two-photon setup. The simulations have been performed for a dye with a two-photon cross section $\delta_2 = 50$ GM (1 GM $= 10^{-50}$ cm^4 s/photons) and a quantum yield $\phi = 0.5$ illuminated with an average power $\langle P\rangle_{ave} = 10$ mW. The results, shown in Fig. 8 indicate that, at least under the simplifying assumption that the heat dissipation occurs completely in air, the temperature increase is relatively high and comparable to the limit values of the temperatures T_0 (see Fig. 7) below which fluorescence can be observed. The heat relaxation times for air and glass are $\tau_{xy} \cong 1$ μs and $\tau_{xy} \cong 0.015$ μs, respectively. However the curves in Fig. 8 are well described for $t > 1$ s by an exponential growth, with a characteristic time $\cong$10 s (see solid line in Fig. 8). Because it is difficult to model the interactions of the molecule with the glass substrate, we can imagine that the actual increase in the temperature lies between the two extremes obtained for the dissipation in air or in water. In any case we could predict an increase of several degrees in the local temperature depending on the excitation power and the quantum yield. Fig. 8 shows that the temperature increases rapidly toward an asymptotic value at high temperature. This finding, compared to the experimental values of the bleaching time that can reach several tens of seconds, may suggest that the transition to the putative dark state does not occur right after the molecule has reached a threshold temperature and that the molecular structure needs some finite time to make the transition to the new electronic dark state after exploring different conformational states.

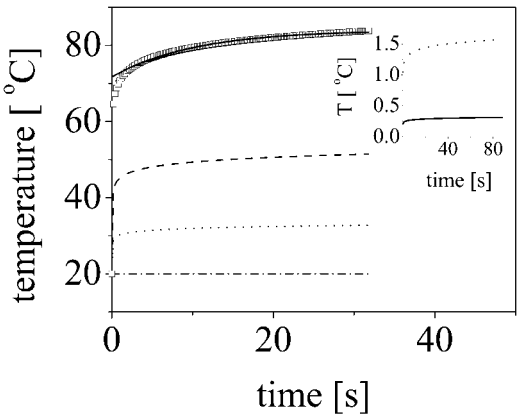

FIGURE 8 Temperature increase as simulated for the two-photon absorption by means of Eq. 10 in the text for the case $\delta_2 = 50$ GM, $\phi = 0.5$, $\langle P\rangle_{ave} = 10$ mW, $w_0 = 0.22$ μm and $z_0 = 0.66$ μm and for the values of the heat conductivity: $\chi = 4 \times 10^{-6}$ Kcal/sm°K (□), $\chi = 4 \times 10^{-6}$ Kcal/sm°K (*dashed line*), $\chi = 10^{-5}$ Kcal/sm°K (*dotted line*) and $\chi = 4 \times 10^{-4}$ Kcal/sm°K (*dot-dashed line*). The solid line is an exponential growth fit to the case $\chi = 4 \times 10^{-6}$ Kcal/sm°K for $t > 1$ s. Inset: Simulations for the case of single photon absorption by water, $\delta_1 = 10^{-24}$ cm^2, $\chi = \chi_{water} = 4 \times 10^{-4}$ Kcal/sm°K and $\langle P\rangle_{ave} = 10$ (*solid line*) and 50 mW (*dashed line*).

According to the thermal bleaching model, after the molecule drops into a dark state where its cross section is much lower than in the initial ground state, the temperature decreases with time according to Eq. 8 because then no heat is absorbed. Obviously this assumption is an oversimplification because the so-called dark state may still absorb light but with much lower two-photon cross section that implies that the local temperature increases at a much lower rate. On the other hand the heat diffusion times, τ_{xy} or τ_z, are of the order of microseconds or even less and therefore the local temperature must decrease to room temperature very rapidly. This prediction would be inconsistent with the observed dark times $T_D \cong 30$–40 s, if we simply assumed that T_D is the time needed to the molecule to reach a lower temperature at which it can convert back to the ground state S_0. One possible explanation for this behavior is that, for the B-S_0 conversion to take place, the molecule must reach a lower temperature and then a finite time is required to explore the possible conformational states. Moreover the hydration shell continuously absorbs IR radiation, although to a very limited extent because $\delta_1 \cong 10^{-24}$ cm^2 (Hale and Querry, 1976), and this may hinder and slow down the heat dissipation of the molecule even after the transition to the dark state B has occurred. A simple simulation gives a maximum increase in the temperature of $\cong$1.6°C for an average excitation power $\langle P\rangle_{ave} = 50$ mW and $\cong$0.3°C for $\langle P\rangle_{ave} = 10$ mW, as shown in the inset of Fig. 8. This tiny increase in temperature of the hydration water is probably not large enough to induce a reduced heat diffusion time, τ_{xy} and τ_z, from the molecule.

On the other hand a further indication that the cooling relaxation time τ_C is of the order of a few seconds comes from an analysis of the fluorescence kinetics observed under intermittent illumination. If we assume an exponential growth of the local temperature with warming up time τ_W, followed by a hyperbolic relaxation as indicated by Eq. 8, we can predict a temperature increase after n illumination cycles (of duration $\tau_D + \tau_I$):

$$T_n = T_R + n(T_\infty - T_R)\frac{(1-\exp[-\tau_I/\tau_W])}{(1+\tau_D/\tau_C)}, \qquad (11)$$

where T_R and T_∞ are the room temperature and the limiting temperature reached upon warming up, respectively. The number of cycles n^* needed to reach the value of the temperature that allows the molecule to make the transition to the B state, must be proportional then to the ratio $(1+\tau_D/\tau_C)/(1-\exp[-\tau_I/\tau_W])$, and the bleaching time $T_{BR} = n^*\tau_I$. The increase of T_{BR} with τ_D is therefore:

$$B_R = \frac{\partial}{\partial\tau_D}T_{BR} = \tau_I\frac{\partial}{\partial\tau_D}n^* = \frac{\tau_I}{\tau_C}(1-\exp[-\tau_I/\tau_W])^{-1} \cong \frac{\tau_W}{\tau_C}, \qquad (12)$$

where we have assumed that $\tau_I \ll \tau_W$, which seems to be the case because $\tau_I \cong 0.6$ s and $\tau_W \cong 10$ s (see fit in Fig. 8). Because B_R varies in the range 0.2–3 for the four dyes, we can infer that the cooling time is of the order of the warming time, i.e., lies approximately in the range 0.1–10 s. Apart from the above suggestions, we have no direct and simple explanation for such a long cooling time as can be inferred from the analysis of our data.

The simulations reported above for the temperature increase of the molecule and the hydration water can help understanding the behavior of the thermal bleaching at different substrate temperature for all the dyes. The higher is the starting substrate temperature, the lower is the local temperature jump that must be made for the molecule to fall into the B state. In particular for pyrene, for which the limiting temperature, T_0, seems to be very close to the room temperature, $\cong$21°C, any small increase of the local temperature, such as that predicted for the water shell, would be enough to bring the molecule into the B state or to keep it from a conversion back from the B to the S_0 ground state. This is also in agreement with the fact that for pyrene we could not observe, at room temperature, any fluorescence recovery after the first thermal bleaching (on a sample of $\cong$ 80 molecules) because the local environment is probably at $T > T_0$ due to the water absorption alone. We believe that although on a semi-quantitative basis, these theoretical considerations indicate that the thermal bleaching hypothesis with a $S_0 \longrightarrow B$ transition is compatible with the physical-chemical parameters of the two-photon absorption of the dyes.

We expect therefore to find a common description of these observations by considering the amount of IR light absorbed that is not radiated back. This quantity must be proportional to the product of the single molecule cross section immobilized on the glass surface, $\tilde{\delta}_2$, times the fraction of the absorbed photon pairs that are not converted in fluorescence photons. This second parameter is given by $1-\phi$, where ϕ is the quantum yield. We assume here that the quantum yield of the excited singlet state of the four dyes is the same as that obtained by single photon excitation and reported in the literature (see Table 1). On the other hand, the two-photon cross section of the single molecules, $\tilde{\delta}_2$, cannot be inferred from the literature data that report bulk measurements in solution and we must rely on the fluorescence response to the excitation power determined on the single molecules on the substrates. Because the parameter A_{EXC}, retrieved from the square law fit of the data taken on single molecules, is proportional to $\tilde{\delta}_2\phi$, we take the product $\Sigma = A_{EXC}(1-\phi)/\phi$ as a measure of the amount of the excitation power that is not radiated back as fluorescence by single dyes on the glass slides. The values of Σ are reported in Fig. 9 below the structure of each dye. The bleaching of the dyes observed here is correlated to Σ in many ways. First, the best fit curvature, B, of the bleaching rate increases with Σ while the exponent, C, decreases (see Fig. 9). The

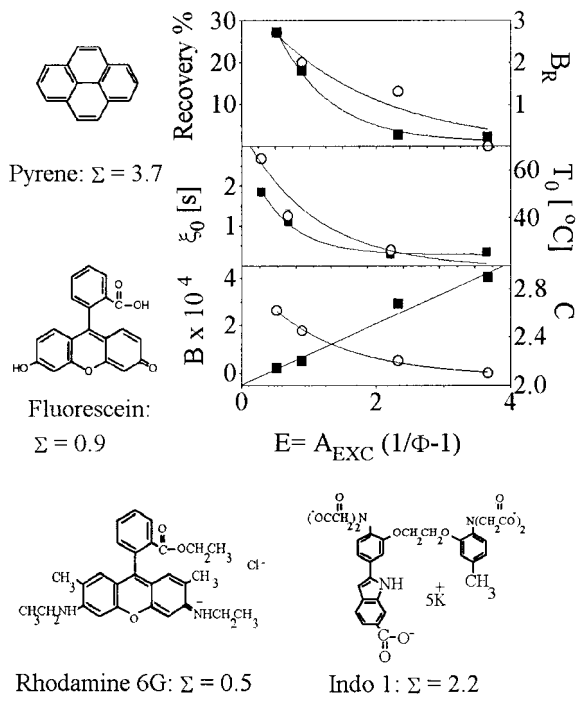

FIGURE 9 Correlation plot of the best fit parameters with the amount of excitation power not reradiated, $\Sigma = A_{EXC}(1-\phi)/\phi$. Upper panel: Left axis, % of the fluorescence recovery at 10 mW; right axis, slope B_R of the bleaching time upon intermittent illumination, T_{BR}, versus the dark time τ_D (see Fig. 6); middle panel: left axis, slope of the bleaching times of small aggregates versus the aggregation order (see text), ξ_0; right axis, temperature T_0 at which no fluorescence can be detected (see Fig. 7); lower panel: left axis, bleaching rate amplitude, B; right axis, bleaching rate exponent, C. The bleaching rate was fit to the law $B \times \langle P \rangle_{ave}^{C}$. In all the panels, the lines are exponential fits intended only to guide the eye. The chemical structures and the values of Σ for the four dyes are reported on the side and below the graphs.

behavior shown by B can be ascribed to a faster increase of the bleaching with $\langle P \rangle_{ave}$ for those dyes that dissipate less radiative energy. The analysis of the trend of the exponent C, that varies in the range 2.1–2.6, is more delicate. The raw data would suggest that the process involves more than two photons for rhodamine 6G, because $C \cong 3$, while for pyrene only two photons are needed. Similar observations have been reported by Patterson and Piston (2000) for two-photon bleaching of fluorescein and indo-1 on microdroplets immobilized between glass slides. The authors reported a somewhat steeper dependence of the bleaching rate upon the excitation power with an exponent $\cong 3$. They ascribed tentatively this behavior to a sequential excitation of the dye in the excited state by a third photon as also indicated for rhodamines by Widengren and Rigler (1996) and Sanchez et al. (1997). However the data reported by Patterson and Piston (2000) could not definitely confirm this model and the authors indicate the possibility of higher resonance absorption.

Also the percentage of the recovery of the fluorescence signal depends monotonically on Σ (Fig. 9, *upper panel*). The observed decrease indicates that an efficient conversion of the excitation power into molecular vibrations leads to dark states so far from the ground state S_0 that it is difficult for the molecule to retrieve it. This observation supports therefore the existence of a family of dark states. Finally the slope, B_R, of the bleaching time versus the dark time in the intermittent illumination experiments (Fig. 9, *upper panel*) is found to decrease with Σ. From the analysis of the temperature increase upon intermittent illumination reported above (see Eqs. 11 and 12) it is clear that the increase of the T_{BR} with τ_D is the more efficient the smaller is the rate of increase of the local temperature of the molecule, i.e., $1/\tau_W$, that is by definition related to the parameter Σ. Finally we notice from Fig. 9 that the parameter Σ does not parallel the complexity of the chemical structure. We try here to define the complexity of the dyes in connection to their possibility to undergo a structural transition. Pyrene is the most rigid structure among those investigated here. Fluorescein and rhodamine 6G are very similar with a rigid structure composed of three condensed rings connected to a benzene ring by a simple C-C bond that allows certain degrees of rotation. Moreover rhodamine 6G has further rotational degrees of freedom in the alkyl groups CH_3CH_2- e CH_3-. These two dyes are characterized by very similar Σ values, $\Sigma \cong 0.5$–0.9, which are much lower than that of pyrene, $\Sigma \cong 3.7$. However for indo-1, whose structure is by far the most complex being characterized by an indole group and two benzene rings connected by simple bonds around which the rotation is allowed, we compute $\Sigma \cong 2.3$. Therefore the chemical structure alone can hardly help in predicting the bleaching property of the dyes. Moreover the good description of the data in terms of the fraction of the absorbed power not going into radiative processes, Σ, appears to support our assumption that the contribution of the vibrational relaxation occurring in the excited state is negligible.

The kinetics of the aggregates call for a separate set of considerations. The multistep decay of the fluorescence is a further indication of the single molecule level of the present measurements. The spread in the bleaching times within each aggregate is definitely larger than the width of the Gaussian distribution found for the single molecules. This fact suggests that the excitation power absorbed by the molecules is not equally distributed over molecular vibrations in the aggregate. Molecules in the aggregate may easily show a different quantum yield due to molecular interactions that opens new deexcitation channels. Therefore the observed spread might be due to slightly different values of Σ for the different monomers in the aggregates. This also correlates with the finding that the spread in the bleaching times in an aggregate increases with the number of aggregation. The larger the number of monomers, the larger is the number of possible interactions that lead to slightly different values of Σ.

CONCLUSIONS

We have presented some evidence that two-photon excitation bleaching at the high excitation intensities needed for single molecule experiments is due to thermal effects. The main cause might be an increase of the local temperature due to the two-photon absorption of the molecules that, being in air, cannot easily dissipate the absorbed heat. The molecular parameter that seems to rule this phenomenon is the amount of absorbed power that is not reradiated as computed on the molecules adsorbed on the glass substrates. These observations shed some light on the bleaching induced by two-photon excitation in single molecule experiments when the molecules are trapped onto solid matrices or three-dimensional structures (e.g., gels). Moreover these data suggest that to increase the number of fluorescence photons per single molecule upon two-photon excitation hydrated samples are more convenient because they can more easily dissipate the thermal loads. Preliminary results on labeled proteins on glass surfaces, in wet silica gels and in trehalose glasses indicate an increase in the thermal bleaching time from the glass surfaces to the wet environment. We suggest therefore that the reduced observation window for single molecules upon two-photon excitation is linked more to the dissipation channels of the absorbed power of the excited molecules rather than to the immobilization on solid substrates. Immobilization procedures, such as wet silica gels, that allow to confine the molecules and to control the hydration of the molecules might therefore be preferable for these types of studies. This systematic study should therefore be extended to different trapping media of interest in single molecule basic research and applications, such as silica or polyacrylamide gels. Finally the observed behavior and the correlations found with the molecular chemical and physical parameters, may be of some help for the design of molecules with switching on-off behavior of longer duration.

APPENDIX

The solution of the diffusion Eq.1 for the two-photon absorption can be obtained by applying the Fourier transform as:

$$\hat{T}\frac{\partial}{\partial t}\Delta\hat{T}(\mathbf{q},t) = -\frac{q^2\chi}{\rho C_P}\Delta\hat{T}(\mathbf{q},t) + V_{EXC}^{0.5}2^{-1.5}\frac{f_{0,TPE}}{\rho C_P}\left[\hat{i}(\mathbf{q})\right]^{0.5}b(t), \tag{4}$$

whose integral is:

$$\Delta\hat{T}(\mathbf{q},t) = \Delta\hat{T}(\mathbf{q},0)\exp\left[-t\frac{q^2\chi}{\rho C_P}\right] + V_{EXC}^{0.5}2^{-1.5}\frac{f_{0,TPE}}{\rho C_P} \times \left[\hat{i}(\mathbf{q})\right]^{0.5}\int_0^t ds\,b(s)\exp\left[-(t-s)\frac{q^2\chi}{\rho C_P}\right] \tag{5}$$

At the time scale of interest here ($\gg 1\ \mu s$) we can assume the laser pulse to be of vanishing width, $b(t) = (2\pi\tau_p^2)^{0.5}\delta(t)$, and obtain:

$$\Delta\hat{T}(\mathbf{q},t) = \left(\Delta\hat{T}(\mathbf{q},0) + V_{EXC}^{0.5}2^{-1.5}(2\pi\tau_p^2)^{0.5}\frac{f_{0,TPE}}{\rho C_P}\left[\hat{i}(\mathbf{q})\right]^{0.5}\right) \times \exp\left[-t\frac{q^2\chi}{\rho C_P}\right] \tag{6}$$

The temperature increase of the molecule can be estimated at $\mathbf{r} = 0$, i.e., at the beam waist, as:

$$\Delta T(0,t) = \int\left(\Delta\hat{T}(\mathbf{q},0) + V_{EXC}^{0.5}2^{-1.5}(2\pi\tau_p^2)^{0.5}\frac{f_{0,TPE}}{\rho C_P}\left[\hat{i}(\mathbf{q})\right]^{0.5}\right) \times \exp\left[-t\frac{q^2\chi}{\rho C_P}\right]d^3\mathbf{q} \tag{7}$$

When the laser first impinges on the sample, the term $\Delta\hat{T}(\mathbf{q},0) = 0$. The laser profile is described by a Gaussian-Lorentzian function, however for the sake of simplification of the computation we assume the laser profile to be approximated by a three-dimensional Gaussian, $i(x,y,z) = \exp\left[-2(x^2+y^2)/w_0^2\right]\exp\left[-2z^2/z_0^2\right]$. The Fourier transform of $i(x,y,z)$ is $i(q_x,q_y,q_z) = V_{EXC}\exp[-(q_x^2+q_y^2)w_0^2/8]\ \exp\left[-q_z^2z_0^2/8\right]$ and the molecule temperature drop, after each laser shot, can be approximated as:

$$\Delta T_{ss}(0,t) = (2\pi)^3(2\pi\tau_p^2)^{0.5}\frac{f_{0,TPE}}{\rho C_P}\left(1+\frac{t}{\tau_{xy}}\right)^{-1}\left(1+\frac{t}{\tau_z}\right)^{-0.5}, \tag{8}$$

where $\tau_{xy} = \rho w_0^2 C_P/4\chi$ and $\tau_z = \rho z_0^2 C_P/4\chi$.

However, because during each image recording the molecule is illuminated for approximately $T_{ON} = 960\ \mu s$ or equivalently for approximately $M = 16{,}000$ shots, the overall temperature increase during the illumination period is:

$$\begin{aligned}\Delta T_{image}^{(on)}(0,T_{ON}) &= \sum_{n=0}^{M}\Delta T_{ss}(0,T_{ON}-n/\nu_p)\\ &\cong \nu_p\int_0^{T_{ON}} ds\,\Delta T_{ss}(0,T_{ON}-s)\\ &= (2\pi)^3(2\pi\tau_p^2)^{0.5}\ \frac{f_{0,TPE}}{\rho C_P}\frac{2\nu_p(\tau_{xy}\tau_z)^{0.5}}{\left(\frac{\tau_z}{\tau_{xy}}-1\right)^{0.5}}\\ &\times\left[Sh^{-1}\left(\left(\frac{\tau_z}{\tau_{xy}}-1\right)^{0.5}\right)\right.\\ &\left.-Sh^{-1}\left(\left(\frac{\tau_z}{\tau_{yx}}-1\right)^{0.5}(1+T_{ON}/\tau_{xy})^{-1}\right)\right]\end{aligned} \tag{9}$$

After the illumination period of $T_{ON} \cong 960\ \mu s$, the molecule is kept in darkness until the next image occurring after $T_{image} \cong 230$ ms, approximately. This implies that the molecular temperature relaxes according to the time dependence of Eq. 8 for each image and for the total acquisition time, $T_{image} = M * 0.23$ s, we obtain:

$$\begin{aligned}\Delta T_{image}(0,T_{image}) &= \sum_{n=0}^{M}\Delta T_{image}^{(on)}(0,T_{ON})\left(1+\frac{t-nT_{image}}{\tau_{xy}}\right)^{-1} \times\left(1+\frac{t-nT_{image}}{\tau_z}\right)^{-0.5}\\ &\cong \Delta T_{image}^{(on)}(0,T_{ON})2\frac{(\tau_{xy}\tau_z)^{0.5}}{T_{image}}\\ &\times\left[Sh^{-1}\left(\left(\frac{\tau_z}{\tau_{xy}}-1\right)^{0.5}\right)\right.\\ &\left.-Sh^{-1}\left(\left(\frac{\tau_z}{\tau_{yx}}-1\right)^{0.5}(1+T_{image}/\tau_{xy})^{-1}\right)\right]\end{aligned} \tag{10}$$

This work was partially supported by grants from the Istituto Nazionale per la Fisica della Materia, Pais SinPhys for the year 2002. We are indebted to Cristiano Viappiani for helpful discussions.

REFERENCES

Brand, L., C. Eggeling, C. Zander, K. H. Drexhage, and C. A. M. Seidel. 1997. Single-molecule identification of Coumarin-120 by time-resolved fluorescence detection: comparison of one- and two-photon excitation in solution. *J. Phys. Chem. A*. 101:4313–4321.

Chirico, G., F. Cannone, S. Beretta, G. Baldini, and A. Diaspro. 2001. Single molecule studies by means of the two-photon fluorescence distribution. *Microsc. Res. Tech*. 55:359–364.

Demas, J. N., and G. A. Crosby. 1971. The measurement of photoluminescence quantum yield: a review. *J. Phys. Chem*. 75:991–1024.

Denk, W., J. H. Strickler, and W. W. Webb. 1990. Two-photon laser scanning fluorescence microscopy. *Science*. 248:73–76.

Denk, W., D. Piston, and W. W. Webb. 1995. Two-photon molecular excitation in laser scanning microscopy. *In* Handbook of Confocal Microscopy. Pawley, J. B., editor. Plenum Press, New York. 445–457.

Diaspro, A. 2002. Confocal and Two-Photon Microscopy, Foundations, Applications and Advances. John Wiley, New York.

Diaspro, A. G. Chirico, F. Federici, F. Cannone, S. Beretta, and M. Robello. 2001. Two-photon microscopy and Spectroscopy Based on a Compact Confocal Scanning Head. *J. Biomed. Opt*. 6:300–310.

Diaspro, A. 2001. Building a two-photon microscope using a confocal laser scanning architecture. *In* Methods in Cellular Imaging. A. Periasamy, editor. Oxford University Press, New York. 162–179.

Diaspro, A., M. Corosu, and M. Robello. 1999. Adapting a compact confocal microscope system to a two-photon excitation fluorescence imaging architecture. *Microsc. Res. Tech*. 47:42–51.

Dickson, R. M., A. Cubitt, R. Y. Tsien, and W. E. Moerner. 1997. On/off blinking and switching behaviour of single molecules of green fluorescent protein. *Nature*. 388:355–358.

Garcia-Parajo, M. F., G. M. J. Segers-Nolten, J. A. Veerman, J. Greve, and N. F. van Hulst. 2000. Real-time light-driven dynamics of the fluorescence emission in single green fluorescent protein molecules. *Proc. Natl. Acad. Sci. USA*. 97:7237–7242.

Hale, M. G., and M. R. Querry. 1976. Optical constants of water in the 200-nm to 200- μm wavelength region. *Appl. Opt*. 12:555–561.

Haughland, R. P. 1996. Handbook of Fluorescent Probes and Research Chemicals. 6th Ed. Molecular Probes Inc., Eugene.

Haupts, U., S. Maiti, P. Schwille, and W. W. Webb. 1998. Dynamics of fluorescence fluctuations in green fluorescent protein observed by fluorescence correlation spectroscopy. *Proc. Natl. Acad. Sci. USA*. 95:13573–13578.

Lu, H. P., and X. S. Xie. 1997. Single-molecule spectral fluctuations at room temperature. *Nature*. 385:143–146.

Mertz, J. 1998. Molecular photodynamics involved in multi-photon excitation fluorescence microscopy. *Eur. Phys. J. D*. 3:53–66.

Patterson, G. H., and D. W. Piston. 2000. Photobleaching in two-photon excitation microscopy. *Biophys. J*. 78:2159–2162.

Pierce, D. W., N. Hom-Booher, and R. D. Vale. 1997. *Nature*. 388: 338–338.

Sanchez, E. J., L. Novotny, G. R. Holtom, and X. S. Xie. 1997. Room-temperature fluorescence imaging and spectroscopy of single molecules by two-photon excitation. *J. Phys. Chem*. 101:7019–7023.

Schönle, A., and S. W. Hell. 1998. Heating by absorption in the focus of an objective lens. *Opt. Lett*. 23:325–327.

Schwille, P., S. Kummer, A. A. Heikal, W. E. Moerner, and W. W. Webb. 2000. Fluorescence correlation spectroscopy reveals fast optical excitation-driven intramolecular dynamics of yellow fluorescent proteins. *Proc. Natl. Acad. Sci. USA*. 97:151–156.

Song, L., E. J. Hennink, I. T. Young, and H. J. Tanke. 1995. Photobleaching kinetics of fluorescein in quantitative fluorescence microscpy. *Biophys. J*. 68:2588–2600.

Song, L., C. A. Varma, J. W. Verhoeven, and H. J. Tanke. 1996. Influence of the triplet excited state on the photobeaching kinetics of fluoresein in microscopy. *Biophys. J*. 70:2959–2968.

Veerman, J. A., M. F. Garcia-Parajo, L. Kuipers, and N. F. van Hulst. 1999. Time-varying triplet state lifetime of single molecules. *Phys. Rev. Lett*. 20:2155–2158.

Wahl, P. 1996. Fluorescence recovery after photobleaching of suspensions of vacuoles. *Biopyhs. Chem*. 57:225–237.

Walser, D., G. Zumofen, A. Renn, and T. Plakhotnik. 2001. Line broadening and line shifts in one- and two-photon single molecule spectra. *J. Phys. Chem. A*. 105:3022–3028.

Weber, W., V. Helms, J. A. McCammos, and P. W. Langhoff. 1999. Shedding light on the dark and weakly fluorescent states of green fluorescent proteins. *Proc. Natl. Acad. Sci. USA*. 96:6177–6182.

Widengren, J., and R. Rigler. 1996. Mechanisms of photobleaching investigated by fluorescence correlation spectroscopy. *Bioimaging*. 4:149–157.

Xu, X., and E. S. Yeung. 1998. Long-range electrostatic trapping of single-protein molecules at a liquid-solid interface. *Science*. 281: 1650–1653.

Xu, C., and W. W. Webb. 1996. Measurements of two-photon excitation cross-section of Molecular fluorophores with data from 690–1050 nm. *J. Opt. Soc. Am. B*. 13:481–491.

Zumbusch, A., and G. Jung. 2000. Single Molecule Spectroscopy of the green fluorescent protein: a critical assessment. *Single Mol*. 1:261–270.